

MIT Open Access Articles

Regime shift of the South China Sea SST in the late 1990s

The MIT Faculty has made this article openly available. **Please share** how this access benefits you. Your story matters.

Citation: Thompson, Bijoy, Pavel Tkalich, and Paola Malanotte-Rizzoli. "Regime Shift of the South China Sea SST in the Late 1990s." *Climate Dynamics* (May 20, 2016).

As Published: <http://dx.doi.org/10.1007/s00382-016-3178-4>

Publisher: Springer Berlin Heidelberg

Persistent URL: <http://hdl.handle.net/1721.1/107387>

Version: Author's final manuscript: final author's manuscript post peer review, without publisher's formatting or copy editing

Terms of use: Creative Commons Attribution-Noncommercial-Share Alike



Regime shift of the South China Sea SST in the late 1990s

Bijoy Thompson¹  · Pavel Tkalich¹ · Paola Malanotte-Rizzoli²

Received: 13 March 2016 / Accepted: 17 May 2016
© Springer-Verlag Berlin Heidelberg 2016

Abstract Decadal variability of the South China Sea (SCS) sea surface temperature (SST) during 1982–2014 is investigated using observations and ocean reanalysis datasets. The SCS SST shows an abrupt transition from a cold-to-warm regime in the late 1990s. Based on the long-term SST variability two epochs are defined, 1982–1996 and 2000–2014 as cold and warm regimes respectively, spanning on either side of the 1997–1999 SCS warming. Despite the occurrence of strong El Niño induced warming events, the SST anomalies tend to be negative in the cold regime. Conversely during the warm regime, the positive SST anomalies have dominated over the La Niña driven cooling events. The cold (warm) SST regime is marked by net heat gain (loss) by the SCS. The long-term variations of net surface heat flux are mainly driven by the latent heat flux anomalies while the short wave flux plays a secondary role. Low-frequency variability of the South China Sea throughflow (SCSTF) appears to be closely related to the SCS SST regime shift. The SCSTF shows reversing trends during the cold and warm epochs. The weakened SCSTF in the warm regime has promoted the SCS warming by limiting the outward flow of warm water from the SCS. Meanwhile, enhanced SCSTF during the cold regime acts as a cooling mechanism and lead to persistent negative SST anomalies. The change in trend of the SCSTF and SST

regime shift coincides with the switching of Pacific decadal oscillation from a warm to cold phase in the late 1990s.

Keywords South China Sea · SST regime shift · South China Sea throughflow · Pacific decadal oscillation

1 Introduction

The heat and freshwater balance of the South China Sea (SCS) is controlled by various regional and global air–sea coupled phenomena including the monsoons in seasonal, El Niño–Southern oscillation (ENSO) in inter-annual and Pacific decadal oscillation (PDO) in decadal time-scales (Wyrski 1961; Qu et al. 2004; Fang et al. 2006; Wang and Wang 2006; Wang et al. 2006a; Swapna et al. 2009; Yu and Qu 2013; Wu 2013; Liu et al. 2014; Thompson and Tkalich 2014; Thompson et al. 2015; Tan et al. 2016). The sea surface temperature (SST) variability over the SCS has profound influence on the weather and climate over the region. Recent studies suggest that rather than acting as a passive receiver of the ENSO induced anomalies, the SCS SST can even trigger the ENSO onset or modulate its evolution through air–sea interaction processes (e.g., Gu et al. 2010). The mechanism suggested for conveying the impact of ENSO on remote ocean basins is the “Atmospheric Bridge” (Klein et al. 1999). Changes in the region of convection and cloud cover due to the atmospheric circulation anomalies associated with the ENSO are considered as the primary processes of this remote influence. Inter-annual variability of the SCS SST is significantly correlated with the ENSO events (Klein et al. 1999; Fang et al. 2006). Highest correlation between the SCS SST and ENSO indices are observed with lags of 5–8 months (Klein et al. 1999; Fang et al. 2006; Thompson and Tkalich 2014).

✉ Bijoy Thompson
bijoymet@gmail.com

¹ Tropical Marine Science Institute, National University of Singapore, Singapore 119222, Singapore

² Department of Earth, Atmospheric and Planetary Sciences, Massachusetts Institute of Technology, Cambridge, MA 02139, USA

The PDO or Inter-decadal Pacific Oscillation is an ENSO-like pattern of air–sea coupled climate variability centered over the mid-latitude Pacific Ocean. The warm or positive PDO episodes are featured by cool SSTs in the west Pacific and warm SSTs in the east while the opposite pattern occurs during the cold or negative phase (Mantua et al. 1997). Several regimes of warm/cold phase shift are evident in the PDO during the twentieth century. The past century witnessed roughly two warm phases (1924–1945, 1977–1998) and three cold phases (1890–1923, 1946–1976 and 1999–2014, still continuing). The shifts in warm/cold phases of the PDO cause abrupt changes in the SST, land surface temperature, surface pressure and precipitation over many regions (Dong and Dai 2015). The PDO is suggested to be the dominant mechanism responsible for the decadal and inter-decadal variability of air–sea parameters in the Indo-West Pacific region (Dong and Dai 2015). The earth's climate has subjected to several abrupt regime shifts in the past century. Most recent regime shift in the global climate was observed in 1999 coinciding with the switching of PDO to a negative phase. Significant changes in the East Asian summer monsoon (EASM), EASM–ENSO relationship and SCS sea surface height have been observed since the late 1990s (Zhou et al. 2007; Zhu et al. 2011, 2015; Si and Ding 2013; Song and Zhou 2015; Pei et al. 2015). The EASM and ENSO have exhibited a strong correlation during 1979–1999. Meanwhile, the correlation has been significantly weakened since 1999. The differences in EASM–ENSO relationship during the epochs 1977–1998 and post-1999s are suggested to be caused by the influence of PDO on the El Niño decay speed (Song and Zhou 2015). The decay of El Niño is found to be slower during the positive phase of PDO and faster during the negative phase. Further, the varying El Niño decay speed induces different EASM anomalies by modifying the tropical wind patterns (Feng et al. 2014).

Bathymetry of the SCS is extremely complex due to the presence of shallow sea-shelves and several passages connecting it to the adjacent oceans/seas (Fig. 1). In the south, the Malacca and Karimata Straits connect the SCS to the Andaman and Java Seas respectively. While the Mindoro and Balabac Straits open to the Sulu Sea in the east, the Luzon and Taiwan Straits provide pathways for water mass exchange to the west Pacific Ocean in the northern SCS. Among these the Luzon Strait is the only passage that allows deep-water exchange with the SCS. The Pacific Ocean water entering through the Luzon Strait leaves the SCS by the Taiwan, Mindoro–Balabac, Malacca and Karimata Straits. This complex current system is known as the South China Sea throughflow (SCSTF). The SCSTF acts as an effective cooling mechanism by transporting the surface net heat gain from the SCS (Fang et al. 2009). Qu et al. (2006) suggested that the SCSTF could be considered as

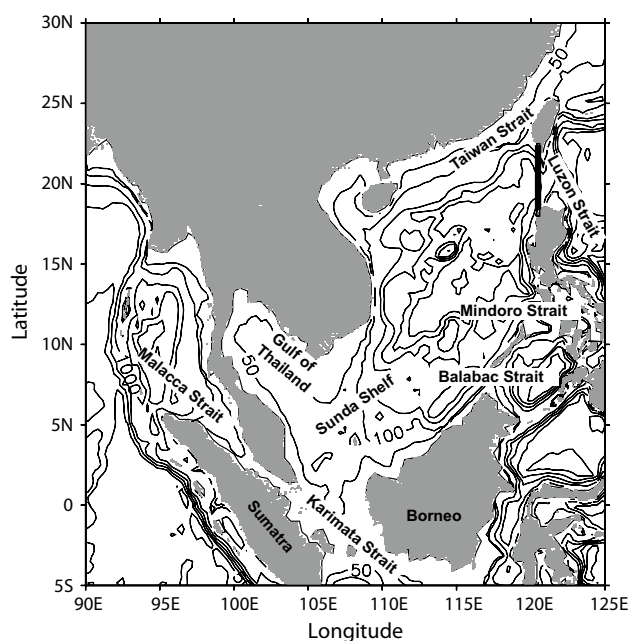


Fig. 1 Bathymetry of the SCS. The LST is computed as the net flow across 120.5°E

a conveyor belt transferring heat and freshwater from the SCS to the surrounding seas. In the annual mean though the Luzon Strait transport (LST) carries relatively warm water from the western Pacific into the SCS, the water exiting from the SCS in the south is even warmer by about 1.8 °C. A large part of the subsurface water entering through the Luzon Strait upwells to the surface layers, gets heated and then flows out of the SCS. The changes in ocean circulation and sea level associated with the monsoons are identified as the primary forcing mechanism of the SCSTF seasonal variability (Metzger and Hurlburt 1996). Meanwhile, its inter-annual as well as decadal variability are considered to be mainly governed by the ENSO Phenomenon (e.g., Qu et al. 2004; Wang et al. 2006b; Liu et al. 2012). However, recent studies revealed that other large-scale phenomena such as the PDO also have a significant role in determining the low-frequency variability of the SCSTF (Yu and Qu 2013; Nan et al. 2015).

Present study investigates the transition of the SCS SST to a warm regime in the late 1990s and related processes. Though the inter-annual SST variability over the SCS is well addressed, to the best of our knowledge, the SST regime shift in the late 1990s is relatively less explored. Yun et al. (2010) have reported an abnormal SST warming over the western Pacific after 1997/1998. Since their focus was to understand the decadal changes of the Asian summer monsoon, detailed examinations of the SST change are not included in the study. One of the strongest El Niño events in recent history was recorded in 1997–1998.

Associated with 1997–1998 El Niño, the SCS has experienced an unprecedented basin-wide warming (Wang et al. 2002). Warm SST anomaly in the SCS started around the middle of 1997 and persisted till mid-1999. While peak of the SST warming is observed in the summer of 1998. Our analysis reveals that the SCS SST exhibits a marked cold-to-warm regime shift after the basin-wide warming related to the 1997/1998 El Niño event. Hence, here we defined two epochs spanning on either side of the 1997–1999 SCS warming; i.e., between 1982 and 1996 (the cold regime) and between 2000 and 2014 (the warm regime). The study aims to present a comprehensive discussion of the SCS SST variability during the cold and warm regimes. To begin with, brief descriptions of the SCS SST seasonal variability is presented. Using observational and re-analysis datasets the role of air–sea heat fluxes and ocean advection on the SST regime shift is investigated. The linear trends of SST and air–sea heat fluxes display distinct features between the cold and warm regimes. The variability of SCSTF related to this regime shift is also examined. Further, the influence of PDO on this cold-to-warm SST regime shift and possible mechanisms are investigated.

2 Data

The atmosphere or ocean re-analysis data products are mostly used for understanding the decadal and inter-decadal climate variability. Due to the extensive assimilation of satellite observations, the re-analysis data may exhibit spurious changes across the 1970s (Xie et al. 2010). Since the present study is limited from 1982, which is roughly coinciding with the advent of satellite SST observations, we believe that possibility for the occurrence of any such erroneous signal will be minimum. The National Oceanic and Atmospheric Administration (NOAA) Advanced Very High Resolution Radiometer (AVHRR) pathfinder satellite series provide an unbroken and high resolution (4 km) SST observation since late 1981. For understanding the SCS SST variability, the NOAA daily Optimum Interpolation Sea Surface Temperature (AVHRR OISSTv2) is used in this study. The spatial resolution of the data is $0.25^\circ \times 0.25^\circ$. In addition to AVHRR satellite data, the SST data is constructed by combining observations from different platforms, including the ships and buoys, on a regular global grid (Reynolds et al. 2007).

The ocean surface heat flux components from the National Oceanography Centre (NOC) flux dataset v2.0 (Berry and Kent 2009, 2011) are employed in the SST budget analysis and for understanding decadal variability of air–sea fluxes over the SCS. NOC flux data provide latent heat flux, sensible heat flux, net long wave and net short wave radiation on a $1^\circ \times 1^\circ$ monthly mean grid for

the global ice-free ocean. Estimate from satellites data, International Comprehensive Ocean Atmosphere Data in situ observations, and numerical models values are used for building the data. The air–sea heat fluxes from 1982 to 2014 are employed in the analysis.

Surface and subsurface current fields from the Simple Ocean Data Assimilation (SODA) v2.2.4 re-analysis are used for understanding the SCSTF variability. The ocean model employed in SODA re-analysis is based on Parallel Ocean Program with an average horizontal resolution of $0.4^\circ \times 0.25^\circ$ and with 40 vertical levels. The assimilated observational data include all available hydrographic profile data as well as ocean station data, moored temperature and salinity time series, surface temperature and salinity observations of various types, and infrared satellite data (Carton and Giese 2008). SODA re-analysis is available in $0.5^\circ \times 0.5^\circ$ horizontal grid in monthly-averaged form during 1871–2008. For consistency, the current fields from 1982 to 2008 are used in the present analysis.

3 Results and discussion

3.1 Seasonal evolution of SST over the SCS

The seasonal variability of SST over the SCS has been discussed in several previous studies (e.g. Chu et al. 1997; Qu 2001; Chen et al. 2003). The spatial distribution of annual SST climatology computed from the OISSTv2 dataset for the period 1982–2014 is shown in Fig. 2a. In the annual climatology, the isotherms are oriented along an axis in northeast to southwest direction. The SST decreases from $\sim 29^\circ\text{C}$ in the southern SCS to less than 26°C in the north. Seasonal variability of the SCS SST is larger over the northern SCS regions where the standard deviation exceeds 2°C (Fig. 2b). Meanwhile, the SST seasonal variability is less than 1°C in the Gulf of Thailand and in the south and eastern regions of the SCS. Though SST over the SCS exhibits significant seasonal variations under the influence of local monsoon systems, the spatial distribution of annual mean SST pattern is dominantly determined by the northeast monsoon (November–February). Relatively high SST standard deviation over the south off Vietnam is related to the existence of a winter cold tongue during the northeast monsoon period (Liu et al. 2004; Thompson et al. 2015). Further to illustrate its meridional variation, zonal average of the SCS SST monthly climatology is shown in Fig. 2c. During the period from December to February, two prominent cooling patterns are observed in the regions 4°N – 10°N and north of 16°N . These SST cooling patterns are driven by the northeast monsoon and seasonal March of the sun. The SST decrease south off Vietnam (4°N – 10°N) is mainly forced by the reduction in net surface heat flux and cold

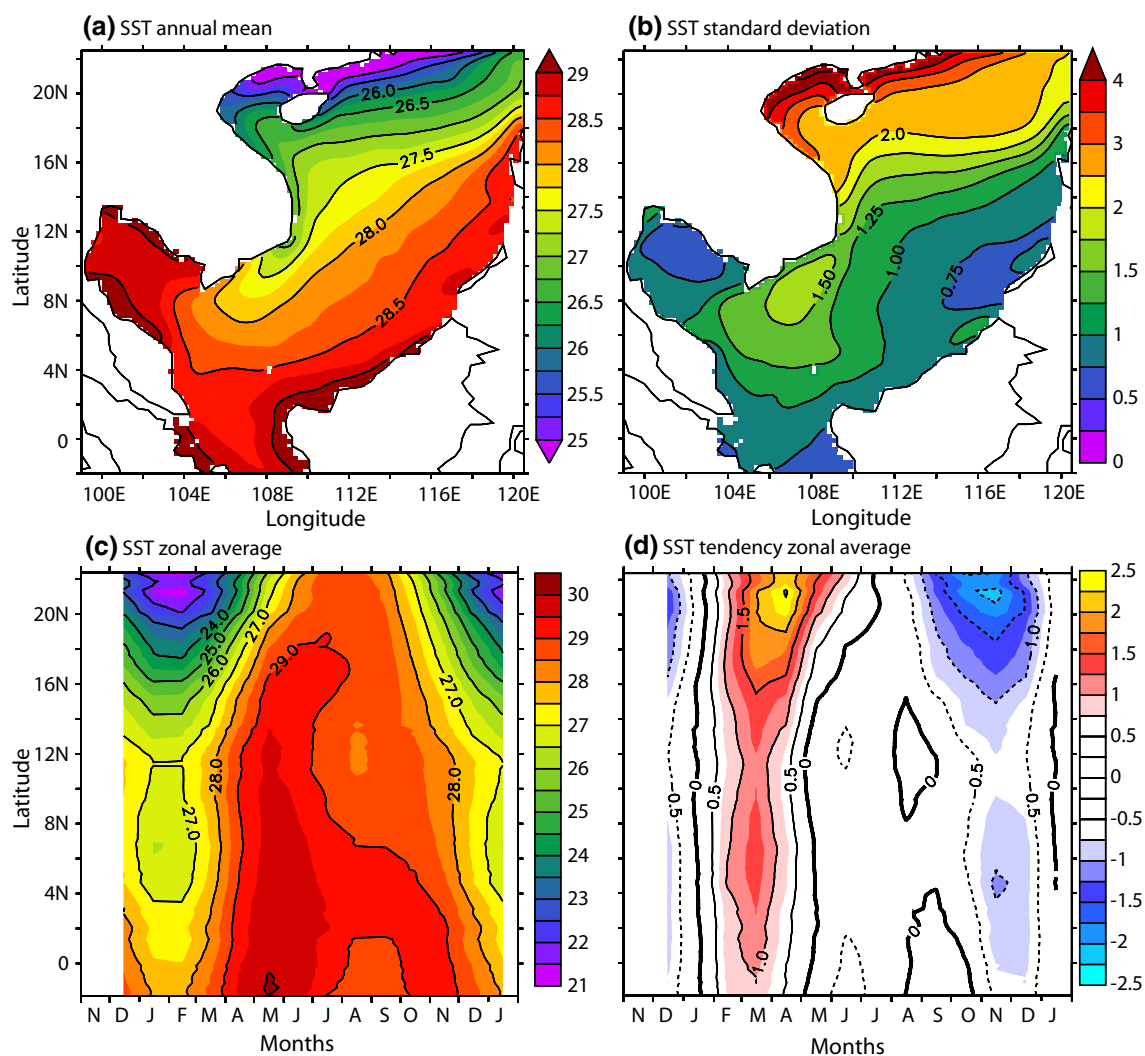


Fig. 2 **a** SST annual mean, **b** SST standard deviation, **c** SST zonal average and **d** Zonal average of SST tendency ($^{\circ}\text{C}$ per month) over the SCS from OISSTv2. The climatology is computed for the period 1982–2014

water advection (Thompson et al. 2015) while the increased release of latent heat flux by strong northeast monsoon winds and decrease in the incoming shortwave flux are responsible for the northern SCS cooling. The warmest surface waters ($>30^{\circ}\text{C}$) in the SCS are encountered near the equatorial region during May. Even the zonally averaged SST is higher than 29.5°C during April–May over the region south of 16°N . The cold water advection associated with the upwelling off the Vietnam coast during the southwest monsoon period (June–September) is reflected as the cooling patch between the region 6°N and 16°N . Further, the SST warming (October–November) associated with withdrawal of southwest monsoon is clearly seen over the region south of 6°N . As evident in the SST standard deviation, the SST tendency is also higher ($>2^{\circ}\text{C}$ per month) over the northern SCS (Fig. 2d). In the northern SCS, the surface temperature shows strong warming and cooling

during April–May and October–December respectively. The SST tendencies are relatively weak over the southern SCS where the SST increases more than 1°C per month during April–May and reduces about 0.5°C per month in November–December.

3.2 SCS SST linear trends and regime shift

Monthly SST anomaly averaged over the SCS from 1982 to 2014 is shown in Fig. 3. To avoid any cold bias in the anomaly, the monthly climatology is prepared after removing the anomalous warming years 1982–1983, 1987–1988, 1997–1999 and 2009–2010. To demonstrate the strength of ENSO events the Nino3.4 index is also plotted in the figure. Inter-annual variability of the SCS SST is closely related to the ENSO events in the Pacific Ocean. Most of the positive peaks in the SST anomaly co-occur with the El

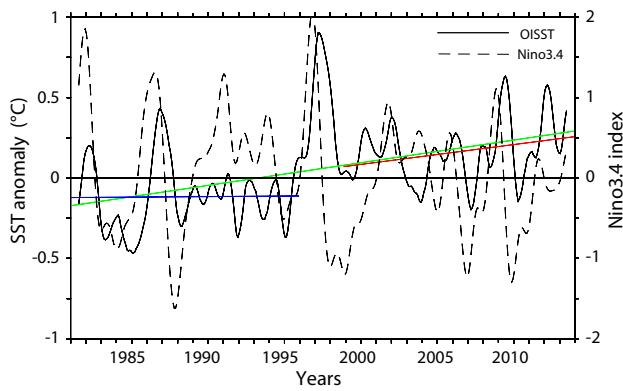


Fig. 3 SST anomaly averaged over the SCS during 1982–2014 overlaid with the Nino3.4 index. *Left* y-axis represent SST anomaly and *right* y-axis indicate Nino3.4 index. The linear trend for the period 1982–2014 (green line), 1982–1996 (blue line) and 2000–2014 (red line) are shown

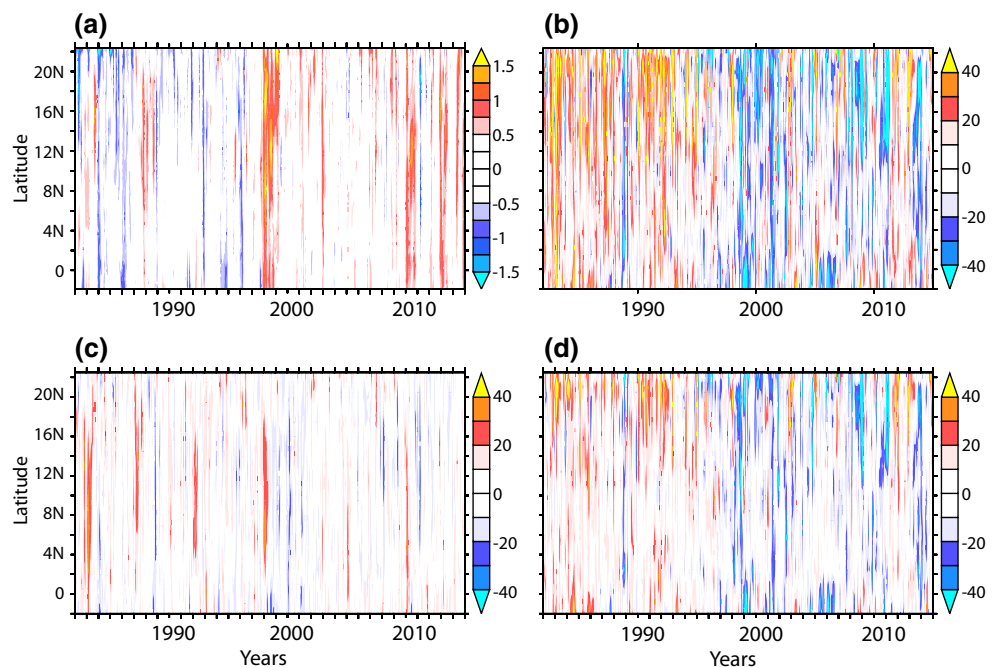
Nino phenomenon. Apart from 1997–1999, significant positive SST anomalies observed in 1982–1983, 1987–1988 and 2009–2010 are associated with strong El Nino events (Fig. 3). Since the response of SCS SST to the ENSO phenomenon is not symmetric (e.g., Wang et al. 2006a), the La Nina related cooling is not evident in some years. For instance, SST cooling is not so obvious during the strong La Nina events in 1988–1989 and 1999–2000.

The SCS SST shows a linear increasing trend in the last few decades. The SST linear trend during 1982–2014 is $0.17\text{ }^{\circ}\text{C}$ per decade (Fig. 3). Interestingly, the basin wide average of SST exhibits a clear distinction in linear

trends pre- and post-years of the SCS warming event in 1997–1999. The SST linear trend in the period 1982–1996 shows relatively low warming rate of $0.10\text{ }^{\circ}\text{C}$ per decade, while the warming rate is considerably accelerated during 2000–2014. The SST linear trend in the later period is about $0.24\text{ }^{\circ}\text{C}$ per decade. Thus, the SCS SST clearly displays transition from a cold-to-warm regime after the warming event occurred in 1997–1999. The spatially averaged SST yields a temperature difference of about $0.4\text{ }^{\circ}\text{C}$ between 1982–1996 and 2000–2014. Prior to 1997, the SST anomalies tend to be in the cold regime except the El Nino induced warming peaks that occurred during the years 1982–1983 and 1987–1988. Post 1997, the SCS SST mostly remains in the warm regime except for a few cooling events occurred in 2004–2005, 2008 and 2011. Among these the later two cooling events co-occurred with the La Nina phenomenon.

For detailed analysis on the spatial extent of the cold-to-warm regime shift in the SCS SST, the zonally averaged SST anomaly is presented in Fig. 4a. The figure clearly demonstrates the dominance of cold and warm SST anomalies in pre- and post-periods of 1997–1999 SCS warming respectively. Also, the cold/warm anomalies are extended over most of the SCS basin. As discussed earlier, the warm/cold anomalies in the cold/warm regimes are mainly related to the El Nino/La Nina events in the Pacific Ocean. The changes in local air–sea interaction processes associated with cold-to-warm SST shift are investigated using the NOC surface heat flux datasets. The zonal averages of net surface heat flux, net shortwave radiation and latent heat flux anomaly are shown in Fig. 4b–d. Since the changes in

Fig. 4 Zonal average of the SST in $^{\circ}\text{C}$ (a), net surface heat flux in w m^{-2} (b), short wave flux in w m^{-2} (c) and latent heat flux in w m^{-2} (d) anomalies over the SCS



net long wave and sensible heat fluxes are relatively weak ($<10 \text{ w m}^{-2}$), those terms are omitted from further analysis. Coherent with SST changes the net surface heat flux also shows strong anomalies. Interestingly, the cold SST regime is characterized by a net heat gain into the SCS and vice versa. The long-term variations of net heat flux are mainly driven by the latent heat flux anomalies. Though the signatures of cold-to-warm climate shift are visible in the short-wave flux anomalies ($\pm 20 \text{ w m}^{-2}$), the variations are not obvious as in the latent heat flux. In the cold regime, the heat gain by the ocean is characterized by an increase in the short wave flux and decrease in latent heat flux release from the ocean. In contrary, enhanced heat loss through the increase in latent heat flux is mainly responsible for the negative heat flux anomalies in the warm regime. A study by Zheng et al. (2015) revealed that the surface wind speed over the SCS shows a linear increasing trend of 3.38 cm s^{-1} per year during 1988–2011. However, the linear trend is observed to be almost negligible from 1988 to 1996. Conversely since 1998, the wind speed shows significant increasing trend and the increase was even rapid in 1998–2003. It is obvious that warm surface temperatures lead to greater release of latent heat flux from the ocean and similar feature observed in different regions of the world oceans (e.g., Rahul and Gnanaseelan 2013). The warm SSTs and increased wind speed are largely responsible for the enhanced heat loss through the latent heat release in the warm regime. Meanwhile, stable winds and cool SSTs are attributed to the positive heat flux anomalies during the cold surface temperature regime.

The linear trend of SST and surface heat fluxes exhibits distinct spatial patterns during the cold and warm regimes. The spatial distribution of linear trends of the SST, net heat flux, short wave and latent heat fluxes in 1982–2014, the cold regime (1982–1996) and the warm regime (2000–2014) are shown in Fig. 5. Over the entire SCS, the SST shows a linear increasing trend during 1982–2014 while an overall decreasing trend is observed in the air–sea heat fluxes (Fig. 5a, d, g, j). The warming rates are higher in the northern SCS and Karimata Strait region and lower in the Gulf of Thailand and south/southeast of Vietnam. The decreasing trend in net heat flux is mainly associated with the enhanced latent heat flux release from the ocean. In the cold regime, significant SST warming rates (>0.01 significance level) are largely limited to the northern SCS and west coast of Borneo (Fig. 5b). Most of the SCS, about 77 % of the total area, is noted by either cooling or insignificant warming trends. In contrast, more than 81 % of the total SCS area is distinguished by significant warming rates during 2000–2014 (Fig. 5c). In the cold regime, following the SST variability, the net heat flux shows relatively high decreasing trend over the regions where the warming is prominent. Meanwhile, low decreasing or positive trends

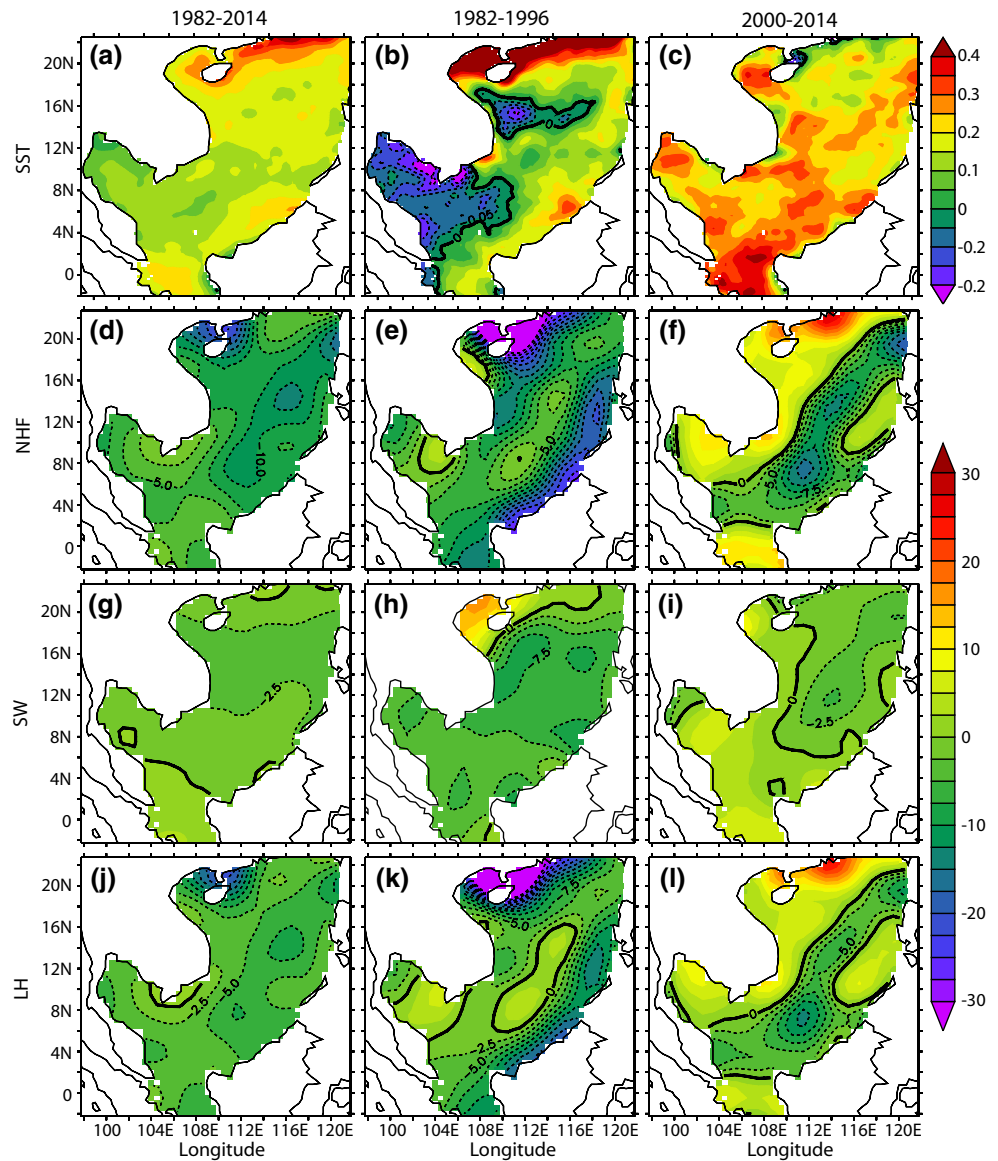
in net heat flux are observed in the regions where the cooling trend is dominant (Fig. 5e). Consistent with our earlier discussions, the spatial pattern of net heat flux linear trend closely follows the latent heat flux variations (Fig. 5k). The SST warming rates tend to be higher in the central and southern SCS in the warm regime (Fig. 5c). Interestingly the northern SCS, where peak warming rates are observed during 1982–1996, is noted by relatively weak warming tendency in the later period. Also, the net heat and latent heat fluxes show a reversal of linear trends while moving from the cold-to-warm regime (Fig. 5f, l). The short wave flux appears to have an important role in the SST warming process during the warm regime. This is illustrated by the presence of short wave flux positive trends in the regions with peak warming rates (Fig. 5i). One remarkable feature in the spatial distribution of net heat and latent heat fluxes is the northeast to southwest orientation of trend lines along an axis connecting the Luzon and Karimata Straits. A similar pattern is seen in the SST linear trend also (Fig. 5c). Essentially, the warm surface temperature is mainly responsible for such a spatial pattern in the net heat flux through enhanced latent heat flux release. Meanwhile, the equatorial SCS, Gulf of Thailand and coasts of Vietnam display quite different behaviors where the short wave flux contribution is dominant.

The analysis suggests that the contribution from net heat flux alone is inadequate to explain the mechanism of SST shift from a cold-to-warm regime and the high warming rates since 2000. Up to a certain extent the increasing trend in shortwave flux could explain the surface temperature warming in the western SCS. The latent heat flux variations appear to be only a passive outcome of the SST warming. The non-linear relationship between the SST and surface heat flux suggests the possible role of ocean dynamics such as advection or SCSTF in the climate shift and warming processes. Since it represents the major pathway of SCSTF, the diagonal orientation of the SST and net heat (latent heat) flux trend further supports this argument. Hence for a detailed analysis, the water mass transport through the Luzon Strait to the SCS (Kuroshio intrusion) and the role of ENSO/PDO on the SST variability is investigated in the following section.

3.3 Implications of the South China Sea throughflow

The water mass transport from the Pacific Ocean to the SCS through the Luzon Strait is the key component of the SCSTF. Since the Luzon Strait is the only deep channel connecting the SCS with the Pacific Ocean, the volume of transport across it is greater compared to the transport through each of the Taiwan, Mindoro-Balabac and Karimata Straits. A modeling study by Yu and Qu (2013) showed that the total volume transports through Taiwan,

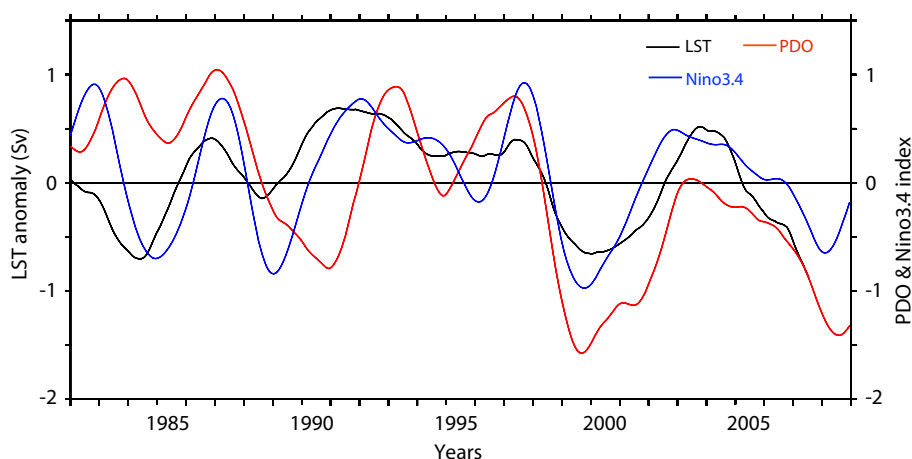
Fig. 5 The linear trends of SST in $^{\circ}\text{C}$ per decade (a–c), net surface heat flux in w m^{-2} per decade (d–f), short wave flux in w m^{-2} per decade (g–i) and latent heat flux w m^{-2} per decade (j–l) over the SCS. The linear trends during 1982–2014, 1982–1996 and 2000–2014 are shown in the left, middle and right panels respectively. The top color bar represents the SST trend while the heat flux trends are indicated by the bottom color bar. The contours represent negative values



Mindoro and Karimata Straits is roughly identical to the LST and hence the changes in LST can be considered as a fair representation of the SCSTF variability. Monthly anomaly of net volume transport (surface to bottom) estimated using SODA through the Luzon Strait between 1982 and 2008 is shown in Fig. 6. A 3-year low-pass filter is applied on the time-series to remove the high frequency oscillations and thus pentadal or higher time-scale variability in the SCSTF will be clearly represented. Positive values indicate strengthening of the LST to the SCS (or westward transport) and vice versa. Low-pass filtered Nino3.4 and PDO indices are also drawn in the figure. The PDO index is defined as the leading principal component of the North Pacific SST variability poleward of 20°N (Mantua et al. 1997). Inter-annual variability of the LST is significantly correlated to the ENSO and generally it leads the

Nino3.4 index. The LST is best correlated when it leads the Nino3.4 index by 2 months (correlation, $r = 0.62$). Meanwhile, this seems to be mostly valid prior to 1996. Inter-annual variations of the LST generally occur in coherent with the Nino3.4 index in the later years. The LST variability is mainly governed by the northward/southward migration of the Pacific North Equatorial Current bifurcation (NECB) latitude during the El Nino/La Nina years (Kim et al. 2004). Northward shift of the NECB during the El Nino years results in weaker Kuroshio Current in east of the Philippines. Subsequent reduction in the potential vorticity enables enhanced penetration of the Kuroshio water through the Luzon Strait (Kim et al. 2004; Qu et al. 2004). Conversely during the La Nina years, the southward shift of the NECB leads to a stronger Kuroshio Current and weaker LST and SCSTF.

Fig. 6 Luzon Strait transport (LST) anomaly computed across 120.5°E (black line) overlaid by the Pacific decadal oscillation (red line) and Niño3.4 index (blue line). A 3-year low-pass filter is applied to the time series. *Left* y-axis represents the LST anomaly while *right* y-axis indicates the PDO and Niño3.4 indices



Recent studies suggest that the PDO plays a dominant role in decadal variability of the LST (Yu and Qu 2013; Nan et al. 2015). The basin-scale wind stress anomalies over the Pacific forced by the PDO influences the NECB latitude and thus modify the LST. During the warm phase of PDO anomalous anticyclonic wind stress over the Philippine Sea push the NECB northward. Eventually, northward shift of the NECB weakens the Kuroshio Current and increases the intrusion of west Pacific water to the SCS through the Luzon Strait. Meanwhile, a weakening of the LST/SCSTF is observed during the PDO cold phase (Yu and Qu 2013). In contrary, as seen in Fig. 6, the LST varies mostly out of phase with the PDO during the years 1982–1995. The poleward shift of Aleutian low and subsequent absence of wind stress curl anomaly over the subtropical region was suggested to be possible reason for this discrepancy (Yu and Qu 2013). Meanwhile after 1995, the decadal variability of the LST is largely following the PDO. This is consistent with the results from recent studies suggesting that decadal variability of the SCS is significantly correlated with the PDO in the last two decades (e.g., Wu 2013; Cheng et al. 2015; Pei et al. 2015). Interestingly, this high correlation period almost coincides with the switching of PDO to a cold phase.

The LST shows a linear decreasing trend (-0.19 Sv per decade, $1 \text{ Sv} = 10^6 \text{ m}^3 \text{ s}^{-1}$) during 1982–2008 (Fig. 6). Meanwhile, a considerable strengthening of the LST (0.54 Sv per decade) is evident in 1982–1996. This suggests a remarkable weakening of the LST/SCSTF in the later years. The linear decreasing trend during 2000–2008 is about -0.7 Sv per decade. Though the LST variability prior to 1997 is not directly correlated with the PDO, its decreasing trend in the post-2000s shows strong association with the PDO. Recent studies emphasizing the enhanced influence of PDO on the SCS decadal variability further supports this argument. Inter-basin pressure gradient between the northwest Pacific Ocean and the SCS is

suggested be an important mechanism influencing the LST and hence the SCSTF. Nan et al. (2013) showed that the pressure gradient between these two basins has a negative trend in last two decades. The basin-mean rate of sea level rise in the SCS during 1993–2012 is 5 mm year^{-1} and about 72 % (3.6 mm year^{-1}) of the total sea level rise is contributed by the PDO (Cheng et al. 2015). The PDO related sea level rise in the SCS might also be responsible for the reduced pressure gradient between the SCS and west Pacific regions. Eventually, this reduced pressure gradient will lead to a weakening of the SCSTF.

The analysis illustrated that the occurrence of cold-to-warm regime shift of the SCS SST and the strengthening/weakening of the SCSTF nearly coincides each other. This suggests the possible influence of SCSTF and hence PDO on the SST regime shift. The strengthened SCSTF during the cold regime assist the SST cooling by transporting more heat out of the basin. Meanwhile, weakening of the SCSTF in the warm regime aids the SST warming by retaining the heat gained from surplus net surface heat flux. Further analysis revealed that the 7-year low pass filtered SST anomaly over the SCS is significantly correlated with the PDO index. The OISSTv2.0 SST anomaly averaged over the SCS and the PDO index shows a correlation of -0.75 during 1982–2014 period.

4 Summary

The SCS is one of the sparsely studied marginal seas in the world due to the scarcity of surface as well as subsurface observations. However, since the beginning of ocean observations from space by remote sensing techniques there have been considerable advancements to our understanding on intra-seasonal to decadal variability of the SCS. The AVHRR-pathfinder series of satellites provide continuous record of SST observation in very high spatio-temporal

resolution since late 1981. Decadal variability of the SCS SST during 1982–2014 is investigated in the study using AVHRR OISSTv2.0 dataset. The SCS SST displays an abrupt transition from a cold-to-warm regime in the late 1990s. The SCS has experienced an extraordinary warming related to the 1997 El Niño event. Warm SST anomaly in the SCS started around the middle of 1997 and persisted till mid-1999. The study shows a clear distinction in the SST linear trends pre- and post-years of the SCS warming in 1997–1999. The SCS SST shows a significant acceleration since 2000 while compared to the warming rate during 1982–1996. Based on the long-term SST variability we defined two epochs 1982–1996 and 2000–2014 as cold and warm regimes respectively, spanning on either side of the 1997–1999 SCS warming. Despite the occurrence of strong El Niño (La Niña) induced warming (cooling) events, the SST anomalies tend to be negative (positive) in the cold (warm) regime.

The role of air–sea heat fluxes and horizontal advection on the SST regime shift are further investigated in the study. The cold (warm) SST regime is marked by net heat gain (loss) by the SCS. Long-term variations of the net surface heat flux are mainly driven by the latent heat flux anomalies while the short wave flux plays a secondary role. Positive surface heat flux in the cold regime is driven by an increase in the short wave flux and decrease in latent heat flux release from the ocean. Whereas enhanced heat loss through latent heat flux is the dominant cause of negative heat flux anomalies in the warm regime. Low-frequency variability of the SCSTF appears to be closely related to the SCS SST regime shift. The LST/SCSTF shows reversing trends during the cold and warm epochs. The SCSTF displays a decreasing trend since the late 1990s. The weakened SCSTF promotes SCS warming by limiting the outward flow of warm water from the SCS. Meanwhile, enhanced SCSTF during the cold regime acts as a cooling mechanism and leads to persistent negative SST anomalies. Change in trend of the SCSTF and SST regime shift coincides with the switching of PDO from a warm to cold phase in the late 1990s. Negative phase change of the PDO weakens the LST/SCSTF by strengthening the Kuroshio Current due to the southward shift of the NECB. Also, the PDO related sea level rise in the SCS reduces the pressure gradient between the SCS and west Pacific Ocean, and thereby weakens the SCSTF. Swapna et al. (2009) investigated the cold/warm regime shift in the SCS associated with the ENSO events during 2000–2003. Weakened LST/SCSTF and changes in air–sea heat fluxes are identified as the major factors responsible for the cold to warm phase shift in their study. The present study suggests that the key processes governing the cold-to-warm regime shift of the SCS SST remains largely unchanged in decadal time scale as well. However, the changes in these processes are found to be dominantly

induced by the PDO rather than the ENSO phenomenon. Results from recent studies illustrating the enhanced correlation between the SCS decadal variability and PDO in the last two decades further supports our findings (Wu 2013; Cheng et al. 2015).

Though there are many studies investigating the decadal shift in the Asian summer monsoon and SCS climate in the late 1990s, the regime shift of SST remains as the least explored. Understanding the characteristics and mechanisms responsible for this cold-to-warm SST regime shift is vital in view of its potential impacts on the climate variability over the Indo-Pacific basin. The present study is important while considering the decadal changes observed in the tropical cyclone activity over the SCS (He et al. 2015), East Asian summer monsoon (Zhu et al. 2011, 2015; Si and Ding 2013) and Indian summer monsoon (Yun et al. 2010) in the late 1990s. The usage of multiple data products has limited our study from presenting a comprehensive discussion about the relative importance of air–sea heat fluxes and SCSTF/PDO on the SST regime shift. Moreover, the spatial resolution of the SODA data is not high enough to well resolve the Mindoro-Balabac and Malacca Straits. Hence the heat and volume transports through these straits are not accurately represented. This has prevented us from presenting the thermodynamic implications of the SCSTF variability on the SST regime shift. More detailed studies employing high resolution coupled climate models are necessary to enhance our understanding on the physical processes and relative contributions of various factors responsible for the SST changes.

Acknowledgments This research was supported by the National Research Foundation Singapore through the Singapore MIT Alliance for Research and Technology's Centre for Environmental Sensing and Modeling interdisciplinary research program. We acknowledge NCDC-NOAA, NOC and UMD for the AVHRR OISSTv2, NOC flux and SODA data sets respectively. The PDO and Niño3.4 indices are obtained from <http://research.jisao.washington.edu/pdo> and <http://climexp.knmi.nl> respectively. Figures are drawn using ferret.

References

- Berry DI, Kent EC (2009) A new air–sea interaction gridded dataset from ICOADS with uncertainty estimates. *Bull Am Meteorol Soc* 90:645–656
- Berry DI, Kent EC (2011) Air–sea fluxes from ICOADS: the construction of a new gridded dataset with uncertainty estimates. *Int J Clim* 31:987–1001
- Carton JA, Giese BS (2008) A reanalysis of ocean climate using Simple Ocean Data Assimilation (SODA). *Mon Weather Rev* 136:2999–3017
- Chen J-M, Chang C-P, Li T (2003) Annual cycle of the South China Sea surface temperature using the NCEP/NCAR reanalysis. *J Meteorol Soc Jpn* 81:879–884
- Cheng X, Xie S-P, Du Y, Wang J, Chen X, Wang J (2015) Interannual-to-decadal variability and trends of sea level in the South China Sea. *Clim Dyn*. doi:10.1007/s00382-015-2756-1

- Chu PC, Lu S, Chen Y (1997) Temporal and spatial variabilities of the South China Sea surface temperature anomaly. *J Geophys Res* 102:20937–20955
- Dong B, Dai A (2015) The influence of the interdecadal Pacific oscillation on temperature and precipitation over the globe. *Clim Dyn* 45:2667–2681
- Fang G, Chen H, Wei Z, Wang Y, Wang X, Li C (2006) Trends and interannual variability of the South China Sea surface winds, surface height, and surface temperature in the recent decade. *J Geophys Res* 111:C11S16. doi:[10.1029/2005JC003276](https://doi.org/10.1029/2005JC003276)
- Fang G, Wang Y, Wei Z, Fang Y, Qiao F, Hu X (2009) Inter-ocean circulation and heat and freshwater budgets of the South China Sea based on a numerical model. *Dyn Atmos Ocean* 47:55–72
- Feng J, Wang L, Chen W (2014) How does the East Asian summer monsoon behave in the decaying phase of El Niño during different PDO phases? *J Clim* 27:2682–2698
- Gu D-J, Li T, Ji Z-P, Zheng B (2010) Connection of the South China Sea summer monsoon to maritime continent convection and ENSO. *J Trop Meteorol*. doi:[10.3969/j.issn.1006-8775.2010.01.001](https://doi.org/10.3969/j.issn.1006-8775.2010.01.001)
- He H, Yang J, Gong D, Mao R, Wang Y, Gao M (2015) Decadal changes in tropical cyclone activity over the western North Pacific in the late 1990s. *Clim Dyn* 45:3317–3329
- Kim YY, Qu T, Jensen T, Miyama T, Mitsudera H, Kang H-W, Ishida A (2004) Seasonal and interannual variations of the North Equatorial current bifurcation in a high-resolution OGCM. *J Geophys Res*. doi:[10.1029/2003JC002013](https://doi.org/10.1029/2003JC002013)
- Klein SA, Soden BJ, Lau N-C (1999) Remote sea surface variations during ENSO: evidence for a tropical atmospheric bridge. *J Clim* 12(4):917–932
- Liu Q, Jiang X, Xie S-P, Liu WT (2004) A gap in the Indo-Pacific warm pool over the South China Sea in boreal winter: seasonal development and interannual variability. *J Geophys Res* 109:C07012. doi:[10.1029/2003JC002179](https://doi.org/10.1029/2003JC002179)
- Liu QY, Huang RX, Wang DX (2012) Implication of the South China Sea throughflow for the interannual variability of the regional upper-ocean heat content. *Adv Atmos Sci* 29(1):54–62
- Liu Q-Y, Wang D, Wang X, Shu Y, Xie Q, Chen J (2014) Thermal variations in the South China Sea associated with the eastern and central Pacific El Niño events and their mechanisms. *J Geophys Res* 119:8955–8972
- Mantua NJ, Hare SR, Zhang Y, Wallace JM, Francis RC (1997) A Pacific interdecadal climate oscillation with impacts on salmon production. *Bull Am Meteorol Soc* 78:1069–1079
- Metzger EJ, Hurlburt HE (1996) Coupled dynamics of the South China Sea, the Sulu Sea, and the Pacific Ocean. *J Geophys Res* 101:12331–12352
- Nan F, Xue H, Chai F, Wang D, Yu F, Shi M, Guo P, Xiu P (2013) Weakening of the Kuroshio Intrusion into the South China Sea over the past two decades. *J Clim* 26:8097–8110
- Nan F, Xue H, Yu F (2015) Kuroshio intrusion into the South China Sea: a review. *Prog Oceanogr* 137:314–333
- Pei Y, Zhang R-H, Zhang X, Jiang L, Wei Y (2015) Variability of sea surface height in the South China Sea and its relationship to Pacific oscillations. *Acta Oceanol Sin*. doi:[10.1007/s13131-015-0773-x](https://doi.org/10.1007/s13131-015-0773-x)
- Qu T (2001) Role of ocean dynamics in determining the mean seasonal cycle of the South China Sea surface temperature. *J Geophys Res* 106:6943–6955
- Qu T, Kim YY, Yaremchuk M, Tozuka T, Ishida A, Yamagata T (2004) Can Luzon Strait transport play a role in conveying the impact of ENSO to the South China Sea? *J Clim* 17:3644–3657
- Qu T, Du Y, Sasaki H (2006) South China Sea throughflow: a heat and freshwater conveyor. *Geophys Res Lett* 33:L23617. doi:[10.1029/2006GL028350](https://doi.org/10.1029/2006GL028350)
- Rahul S, Gnanaseelan C (2013) Net heat flux over the Indian Ocean: trends, driving mechanisms, and uncertainties. *IEEE Geosci Remote Sens Lett* 10(4):776–780
- Reynolds RW, Smith MTM, Liu C, Chelton DB, Casey KS, Schlax MG (2007) Daily high-resolution-blended analyses for sea surface temperature. *J Clim* 20:5473–5496
- Si D, Ding Y (2013) Decadal change in the correlation pattern between the Tibetan Plateau winter snow and the East Asian summer precipitation during 1979–2011. *J Clim* 26:7622–7634
- Song F, Zhou T (2015) The crucial role of internal variability in modulating the decadal variation of the East Asian summer monsoon–ENSO relationship during the twentieth century. *J Clim* 28:7093–7107
- Swapna P, Gan J, Lau A, Fung J (2009) On the warm/cold regime shift in the South China Sea: observation and modeling study. *Deep Sea Res* 56:1039–1056
- Tan W, Wang X, Wang W, Wang C, Zuo J (2016) Different responses of Sea Surface Temperature in the South China Sea to various El Niño events during Boreal Autumn. *J Clim* 29:1127–1142
- Thompson B, Tkalich P (2014) Mixed layer thermodynamics of the Southern South China Sea. *Clim Dyn* 43:2061–2075
- Thompson B, Tkalich P, Rizzoli PM, Fricot B, Mas J (2015) Dynamical and thermodynamical analysis of winter cold tongue in the South China Sea. *Clim Dyn*. doi:[10.1007/s0038201529243](https://doi.org/10.1007/s0038201529243)
- Wang W, Wang C (2006) Formation and decay of the spring warm pool in the South China Sea. *Geophys Res Lett* 33:L02615. doi:[10.1029/2005GL025097](https://doi.org/10.1029/2005GL025097)
- Wang DX, Xie Q, Du Y, Wang WQ, Chen J (2002) The 1997–1998 warm event in the South China Sea. *Chin Sci Bull* 47:1221–1227
- Wang C, Wang W, Wang D, Wang Q (2006a) Interannual variability of the South China Sea associated with El Niño. *J Geophys Res* 111:C03023. doi:[10.1029/2005JC003333](https://doi.org/10.1029/2005JC003333)
- Wang D, Liu Q, Huang R, Du Y, Qu T (2006b) Interannual variability of the South China Sea throughflow inferred from wind data and an ocean data assimilation product. *Geophys Res Lett* 33:L14605. doi:[10.1029/2006GL026316](https://doi.org/10.1029/2006GL026316)
- Wu CR (2013) Interannual modulation of the Pacific decadal oscillation (PDO) on the low-latitude western North Pacific. *Prog Oceanogr* 110:49–58
- Wyrtki K (1961) Physical oceanography of Southeast Asian waters. NAGA Rep 2, Scripps Institution of Oceanography, p 195
- Xie S-P, Du Y, Huang G, Zheng X-T, Tokinaga H, Hu K, Liu Q (2010) Decadal shift in El Niño influences on Indo-Western Pacific and East Asian climate in the 1970s. *J Clim* 23:3352–3368
- Yu K, Qu T (2013) Imprint of the Pacific decadal oscillation on the South China Sea throughflow variability. *J Clim* 26:9797–9805
- Yun K-S, Ha K-J, Wang B, Ding R (2010) Decadal cooling in the Indian summer monsoon after 1997/1998 El Niño and its impact on the East Asian summer monsoon. *Geophys Res Lett* 37:L01805. doi:[10.1029/2009GL041539](https://doi.org/10.1029/2009GL041539)
- Zheng C, Jing P, Yanke T, Zhansheng G, Zhenfeng R, Chaohui C (2015) The seasonal variations in the significant wave height and sea surface wind speed of the China's seas. *Acta Oceanol Sin* 34(9):58–64
- Zhou W, Wang X, Zhou TJ, Li C, Chan JCL (2007) Interdecadal variability of the relationship between the East Asian winter monsoon and ENSO. *Meteorol Atmos Phys* 98:283–293
- Zhu YL, Wang HJ, Zhou W, Ma JH (2011) Recent changes in the summer precipitation pattern in East China and the background circulation. *Clim Dyn* 36:1463–1473
- Zhu Y, Wang H, Ma J, Wang T, Sun J (2015) Contribution of the phase transition of Pacific decadal oscillation to the late 1990s' shift in East China summer rainfall. *J Geophys Res* 120:8817–8827